Double Helix Nodal Line Superconductor

Xiao-Qi Sun, Biao Lian, and Shou-Cheng Zhang

Phys. Rev. Lett. **119**, 147001 — Published 2 October 2017

DOI: 10.1103/PhysRevLett.119.147001

Double helix nodal line superconductor

Xiao-Qi Sun,[1] Biao Lian,[1] and Shou-Cheng Zhang[1]

[1]*Department of Physics, McCullough Building, Stanford University, Stanford, California 94305-4045, USA*

Time-reversal invariant superconductors in three dimensions may contain nodal lines in the Brillouin zone, which behave as Wilson loops of 3d momentum-space Chern-Simons theory of the Berry connection. Here we study the conditions of realizing linked nodal lines (Wilson loops), which yield a topological contribution to the thermal magnetoelectric coefficient that is given by the Chern-Simons action. We find the essential conditions are the existence of torus or higher genus fermi surfaces and spiral spin textures. We construct such a model with two torus fermi surfaces, where a generic spin-dependent interaction leads to double-helix-like linked nodal lines as the superconductivity is developed.

Nodal-line superconductor is an intriguing class of three dimensional (3d) unconventional superconductor that respects time-reversal symmetry. Unlike usual superconductors which are fully gapped, a nodal-line superconductor contains closed gapless nodal lines in the Brillouin zone (BZ), which are protected by time-reversal symmetry. In nature, such superconductors widely occur in cuprates [1–4], iron-based superconductors [5, 6] and noncentrosymmetric superconductors [7, 8]. As 1D loops, the nodal lines in the 3D BZ can form nontrivial links[9–12], where the linking numbers are topologically invariant and give a classification of nodal-line superconductors [9]. Physically, change of linking numbers of nodal lines has been shown to yield a topological shift in the coefficient of thermal magnetoelectric effect, which is also known as the theta angle [9, 13, 14]. This is because the theta angle is theoretically given by the action of the Chern-Simons (CS) theory of Berry connection in the 3D BZ [13], while the nodal lines behave exactly as Wilson loops[9] and linking numbers contribute topologically[15, 16]. On the surface of superconductor, linked nodal lines lead to topologically protected kissing Majorana flat bands which are bounded by the projected nodal lines [17–21]. However, superconductors with linked nodal lines have not been discovered. In this letter, we investigate the physical conditions for realizing linked nodal-line superconductors, and we show the key ingredients for linked nodal lines to occur are torus or higher genus fermi surfaces and certain spiral spin textures. In particular, we construct a double helix nodal-line superconductor lattice model, which contains two pairs of linked nodal lines resembling the DNA double helix structure [22, 23] under the standard BCS mean field theory. Our theory gives a guidance on the search for linked nodal-line superconductors in nature.

Though nodal lines could occur in centrosymmetric TRI materials such as cuprates, they appear more commonly in noncentrosymmetric TRI superconductors, where the electron bands are generically nondegenerate due to spin-orbital couplings (SOCs) [8, 24]. Here we restrict ourselves to the noncentrosymmetric TRI superconductors, which allows us to consider a larger variety of Hamiltonians. Nodal lines are protected by the time-reversal symmetry. Given an electron band of dispersion $\epsilon(\mathbf{k})$ where $\mathbf{k}$ is the lattice momentum, the time-reversal symmetry restricts its pairing amplitude $\Delta(\mathbf{k})$ to be real in a TRI basis [25]. Therefore, the system is gapless when the two conditions $\epsilon(\mathbf{k}) = \Delta(\mathbf{k}) = 0$ are satisfied, which gives rise to one-dimensional nodal lines in the BZ. Note that the nodal lines are restricted on the Fermi surface of the band given by $\epsilon(\mathbf{k}) = 0$, so the fermi surface topology will limit the possible configurations of nodal lines.

It is easy to see that a spherical fermi surface does not support linked nodal lines. While if the fermi surface is a torus, one is able to draw two nodal lines linked with each other along the toroidal direction of the torus, which resembles a closed DNA double helix. An integer Gauss linking number[15, 16, 26] n_L can be defined for such two nodal lines, which is equal to the total number of coils of the double helix (up to a sign). However, one must note the linking number n_L reverses sign under time-reversal transformation, so a double helix cannot be TRI by itself. Instead, the superconductor must contain minimally two double helices which are time reversal partners of each other, and this requires at least two torus fermi surfaces forming a time reversal pair. Fig.1a shows such a configuration of two double helices with linking number $n_L = \pm 1$, respectively, where the two torus fermi surfaces are cylinders periodic in the k_z direction. For fermi surfaces with a higher genus (number of holes) $N_g \geq 2$, it is possible to draw two such double helices on a single TRI fermi surface, and Fig.1d shows such an example. In nature, fermi surfaces with a high genus are quite common in metals.

Given a suitable topology of fermi surfaces, we still need a nontrivial electron-electron interaction to achieve linked nodal lines in the superconductor. Here we take the example of Fig.1a where two cylindrical torus fermi surfaces are centered at $(k_x, k_y) = (\pm Q_x, 0)$, and investigate how the double-helix linked nodal lines of linking number $n_L = \pm 1$ can be realized. The Cooper channel interaction of the superconductor is generically given by $H_I = \sum_{\mathbf{k},\mathbf{k}'}(V_{\mathbf{k}\mathbf{k}'}/2N)c^\dagger_{\mathbf{k}}c^\dagger_{-\mathbf{k}}c_{-\mathbf{k}'}c_{\mathbf{k}'}$, where $c_{\mathbf{k}}$ and $c^\dagger_{\mathbf{k}}$ are the electron annihilation and creation operators at momentum $\mathbf{k}$ near the fermi surfaces, $V_{\mathbf{k}\mathbf{k}'}$ are the interaction coefficients, and N is the number of unit cells. In the presence of time-reversal symmetry, the pairing amplitude $\Delta_{\mathbf{k}} = \langle\sum_{\mathbf{k}'} V_{\mathbf{k}\mathbf{k}'}c_{-\mathbf{k}'}c_{\mathbf{k}'}\rangle/N$ is real. The mean-field free energy of the superconductor is then $F(\Delta_{\mathbf{k}}) = \sum_{\mathbf{k},\mathbf{k}'}(\Delta_{\mathbf{k}}/2E_{\mathbf{k}})V_{\mathbf{k}\mathbf{k}'}(\Delta_{\mathbf{k}'}/2E_{\mathbf{k}'})/2N$, where $E_{\mathbf{k}} = (\epsilon^2_{\mathbf{k}} + \Delta^2_{\mathbf{k}})^{1/2}$ is the Bogoliubov-de Gennes quasiparticle spectrum. Therefore, $\Delta_{\mathbf{k}}$ and $\Delta_{\mathbf{k}'}$ tend to have the same (opposite) sign for $V_{\mathbf{k}\mathbf{k}'} < 0$ ($V_{\mathbf{k}\mathbf{k}'} > 0$). By definition of nodal lines, $\Delta_{\mathbf{k}}$ on a fermi sur-

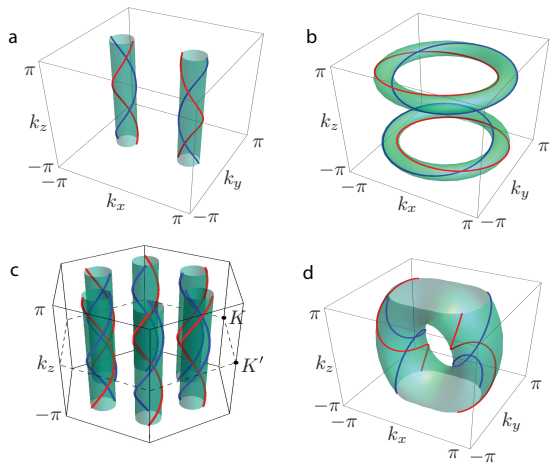

FIG. 1: Examples of fermi surfaces compatible with TRI linked nodal lines. **a**-**c** shows how such linked nodal lines may occur on torus fermi surfaces. **d** shows a possible configuration of linked nodal lines on a genus two fermi surface.

face will take opposite signs on the two sides of a nodal line. For the double helix nodal lines shown in Fig.1a, one finds $\Delta_{\mathbf{k}}\Delta_{\mathbf{k}'} \leq 0$ when $\mathbf{k} - \mathbf{k}' = (0, 0, \pi)$, or when $\mathbf{k}$ and $\mathbf{k}'$ lie in the same plane of constant k_z and opposite to each other on the same cylindrical fermi surface. This motivates us to write down the following interaction for $\mathbf{k}$ and $\mathbf{k}'$ on the same fermi surface:

$$V_{\mathbf{k}\mathbf{k}'} = -\left(\eta_1 \widetilde{k_x}\widetilde{k'_x} + \eta_2 k_y k'_y\right)\cos(k_z - k'_z)\,, \tag{1}$$

where we have defined $\widetilde{k_x} = k_x \mp Q_x$ for momentum $\mathbf{k}$ near $(k_x, k_y) = (\pm Q_x, 0)$, respectively. The interaction at the other momentums can be obtained via the relation $V_{\mathbf{k}\mathbf{k}'} = -V_{\mathbf{k},-\mathbf{k}'} = -V_{-\mathbf{k},\mathbf{k}'}$. We expect the double helix nodal lines with linking number ± 1 to be favored when such a term dominates in the electron-electron interaction near fermi surfaces.

Such a $\mathbf{k}$-dependent interaction can be realized from a spin-dependent Heisenberg interaction together with a spiral fermi-surface spin texture due to SOC. To illustrate this idea, we can start from two spin-degenerate cylindrical fermi surfaces at $(k_x, k_y) = (\pm Q_x, 0)$, and add a SOC as follows:

$$H_{\rm soc}(\mathbf{k}) = \mathbf{g}(\mathbf{k})\cdot\boldsymbol{\sigma} = \lambda(k_y\sigma_x - \widetilde{k_x}\sigma_y) + \lambda_z(\sin k_z\sigma_x \pm \cos k_z\sigma_y), \tag{2}$$

where $\sigma_{x,y,z}$ are the Pauli matrices for spins, the $\pm$ signs correspond to $\mathbf{k}$ near $(k_x, k_y) = (\pm Q_x, 0)$, respectively, and we keep only the leading order expansion in $\widetilde{k_x}$ and k_y. Due to the SOC, the fermi surfaces split into two inner cylinders and two outer ones centered at $(k_x, k_y) = (\pm Q_x, 0)$. In particular, the λ_z term leads to a spiral spin texture on each fermi surface that rotates along the k_z direction. For a generic spin-dependent interaction $H_I = V(\mathbf{r}_1 - \mathbf{r}_2)\rho(\mathbf{r}_1)\rho(\mathbf{r}_2) + J(\mathbf{r}_1 - \mathbf{r}_2)\mathbf{S}(\mathbf{r}_1)\cdot\mathbf{S}(\mathbf{r}_2)$ where $\rho(\mathbf{r})$ and $\mathbf{S}(\mathbf{r})$ are the local electron density and spin operators. The projection onto the spin texture will naturally yield an interaction as shown in Eq.(1), as we will show later.

We also want to mention a different way to understand the linked nodal lines induced by SOC as follows. Generically, the TRI pairing amplitude of the two bands splited by SOC is a matrix in the natural electron spin $s_z = \pm 1/2$ basis as follows [27]:

$$\Delta_{ss'}(\mathbf{k}) = \left\{\left[\psi(\mathbf{k}) + \mathbf{d}(\mathbf{k})\cdot\boldsymbol{\sigma}\right] i\sigma_y\right\}_{ss'}\,, \tag{3}$$

where $\psi(\mathbf{k}) = \psi(-\mathbf{k})$ gives a singlet pairing while $\mathbf{d}(\mathbf{k}) = -\mathbf{d}(-\mathbf{k})$ corresponds to a triplet pairing, both of which are real functions of $\mathbf{k}$. For a system with a SOC given by $H_{\rm soc} = \mathbf{g}(\mathbf{k})\cdot\boldsymbol{\sigma}$, it is shown [28] that the most favorable pairing amplitude satisfies $\mathbf{d}(\mathbf{k}) = \xi(\mathbf{k})\mathbf{g}(\mathbf{k})$, where $\xi(\mathbf{k})$ is a scalar function. This yields a pairing amplitude $\Delta(\mathbf{k}) = \psi(\mathbf{k}) \mp \xi(\mathbf{k})|\mathbf{g}(\mathbf{k})|$ on the two outer ($-$ sign) and inner ($+$ sign) cylindrical fermi surfaces. In the simplest case when both $\psi(\mathbf{k}) = \psi$ and $\xi(\mathbf{k}) = \xi$ are constants, nodal lines will occur at the intersections between the outer cylindrical fermi surfaces and the constant $|\mathbf{g}(\mathbf{k})|$ surfaces defined by $\Delta(\mathbf{k}) = \psi - \xi|\mathbf{g}(\mathbf{k})| = 0$. Fig.2a shows the intersection nodes A, B and A', B' in the $k_z = 0$ plane, where the white circles are the outer cylindrical fermi surfaces, and the yellow loops are constant $|\mathbf{g}(\mathbf{k})| = \psi/\xi > 0$ surfaces, which are centered at Λ and Λ' where $|\mathbf{g}(\mathbf{k})| = 0$. The light (dark) color represents the regions where $|\mathbf{g}(\mathbf{k})|$ is large (small), and the arrows show the spin textures in the BZ. As k_z increases from 0 to 2π, the Λ point moves along a spiral trajectory $\left(Q_x + \frac{\lambda_z}{\lambda}\cos k_z, -\frac{\lambda_z}{\lambda}\sin k_z, k_z\right)$, and similarly for Λ', so the gapless nodes A, B (and A', B') will undergo a 2π rotation with respect to k_z, yielding a double helix nodal line structure. We note that in order to have intersection nodes, the value of ψ/ξ must be within a certain range, which is determined by interactions. Similarly, nodal lines may also occur on the inner fermi surfaces at intersections where $|\mathbf{g}(\mathbf{k})| = -\psi/\xi$ (if $\psi/\xi < 0$), which also form double helices.

Now we rewrite the above model in a 3d lattice, and demonstrate the above interaction and SOC indeed give rise to double-helix linked nodal lines. We assume the following single-electron Hamiltonian with SOC:

$$\begin{aligned} H_0(\mathbf{k}) = {} & t'\cos 2k_x - t\cos k_y + \lambda_1\sigma_x\sin k_y + \lambda_2\sigma_y\sin 2k_x \\ & + \lambda_3\sigma_x\sin k_z + \lambda_4\sigma_y\sin k_x\cos k_z - \mu\,, \end{aligned} \tag{4}$$

where t and t' are positive, and λ_i ($1 \leq i \leq 4$) are SOC parameters which are TRI but inversion asymmetric. When the SOC is zero, the electron kinetic energy has its minima at $(k_x, k_y) = (\pm\pi/2, 0)$. For chemical potential μ satisfying $-t' - t < \mu < -|t - t'|$, the fermi surfaces are two spin-degenerate cylindrical tori centered at the minima. When the SOC is turned on, the fermi surfaces split into two inner tori and two outer tori, and acquire spin textures. For convenience, we fix $\lambda_1 = 2\lambda_2 = \lambda$ and $\lambda_3 = \lambda_4 = \lambda_z$. The SOC reduces to the form of Eq.(2) in the vicinity of $(k_x, k_y) = (\pm\pi/2, 0)$. In principle, the Hamiltonian could contain other hopping or SOC terms, but we will keep them zero since they do not qualitatively change the physics [29]. In the following discussion, we will fix the single-particle parameters at $t' = 0.25t$,

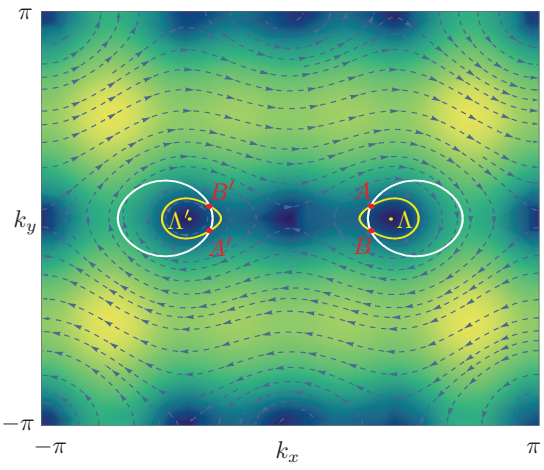

FIG. 2: The arrows show the spin textures of the lower electron band in the $k_z = 0$ plane for $\lambda = -0.02t$, $\lambda_z = 0.005t$, and the brightness is proportional to the SOC strength $|\mathbf{g}(\mathbf{k})|$ (brighter color for larger $|\mathbf{g}(\mathbf{k})|$). In particular, $|\mathbf{g}(\mathbf{k})| = 0$ at Λ and Λ' points. The nodal lines occur at A, B and A', B' points which are intersections between the fermi surfaces as given by the white circles and the constant $|g(\mathbf{k})| = \psi/\xi$ contours (yellow circles).

$\lambda = -0.2t$, $\lambda_z = 0.4t$. For simplicity, we will also fix the chemical potential at $\mu = -1.6t$ slightly above the band minimum, so that the two inner torus fermi surfaces shrink to zero [29], with only the two outer torus fermi surfaces left.

We then add an electron-electron interaction to the system as follows[30]:

$$H_{\text{int}} = \frac{1}{N}\sum_{\mathbf{q}} V(\mathbf{q})\rho_{\mathbf{q}}\rho_{-\mathbf{q}} + \frac{1}{N}\sum_{\mathbf{q}} J(\mathbf{q})\mathbf{S}_{\mathbf{q}}\cdot\mathbf{S}_{-\mathbf{q}}\,, \qquad (5)$$

where $\rho_{\mathbf{q}} = \sum_{\mathbf{k}s} c^{\dagger}_{\mathbf{k}+\mathbf{q},s}c_{\mathbf{k},s}$ and $\mathbf{S}_{\mathbf{q}} = \frac{1}{2}\sum_{\mathbf{k}ss'} c^{\dagger}_{\mathbf{k}+\mathbf{q},s}\boldsymbol{\sigma}_{ss'}c_{\mathbf{k},s'}$ are the electron density and spin operators at momentum $\mathbf{q}$. Such an interaction may generically arise from the phonon exchange and the electron itinerant magnetism. Explicitly, we assume the interaction potentials take the form $V(\mathbf{q}) = V_0 + V_x\cos 2k_x + V_y\cos k_y$ and $J(\mathbf{q}) = J_x\cos 2k_x + J_y\cos k_y$, where V_0, V_x, V_y, J_x and J_y are constants. With the spin textures known, one can readily project the interaction onto the two cylindrical fermi surfaces. Using a $\mathbf{k}\cdot\mathbf{p}$ expansion, one can show the Cooper channel interaction potential $V_{\mathbf{k}\mathbf{k}'}$ for $\mathbf{k}$ and $\mathbf{k}'$ on the same fermi surface is given by [29]:

$$\begin{aligned} V_{\mathbf{k}\mathbf{k}'} &= \eta_0 - \left(\eta_1\widetilde{k}_x\widetilde{k}'_x + \eta_2 k_y k'_y\right)\cos\left[\phi(\mathbf{k}) - \phi(\mathbf{k}')\right] \\ &\quad - \eta_3(\widetilde{k}_x^{\,2} + \widetilde{k}_x'^{\,2}) - \eta_4(k_y^2 + k_y'^2)\,. \end{aligned} \qquad (6)$$

where we have kept terms up to the second order in $\widetilde{k}_x$ and k_y. Here $\phi(\mathbf{k})$ is the angle of the spin direction at $\mathbf{k}$ in the k_x-k_y plane, $\eta_1 = -(4V_x + J_x)$, $\eta_2 = -(V_y + J_y/4)$, $\eta_3 = 2V_x - 3J_x/2$, $\eta_4 = V_y/2 - 3J_y/8$, $\eta_0 = V_0 + \eta_3/2 + 2\eta_4$, and we have $\widetilde{k}_x = k_x \mp \pi/2$ for momentum near $(k_x, k_y) = (\pm\pi/2, 0)$, respectively. Compared with Eq.(1), the above interaction contains a few other less important terms and has the spin angle $\phi(\mathbf{k})$ in place of k_z. However, since the spin angle $\phi(\mathbf{k})$ increases(decreases) by 2π as k_z goes from $-\pi$ to π on the two fermi surfaces, the above interaction still satisfies the condition for double helix nodal lines. Based on this interaction near fermi surfaces, we solve numerically the linearized gap equation that determines the mean-field superconductivity critical temperature T_c [30]:

$$-\chi\Psi(\mathbf{k}) = \frac{1}{2N\epsilon_c}\sum_{\mathbf{k}'} V_{\mathbf{k}\mathbf{k}'}\Psi(\mathbf{k}')\,, \qquad (7)$$

where ϵ_c is the interaction cutoff energy (e.g. Debye energy), $\mathbf{k}$ is summed within the energy shell $[-\epsilon_c, \epsilon_c]$ near the fermi surface, while $\Psi(\mathbf{k}) \propto \Delta(\mathbf{k})$ is an eigenvector of $V_{\mathbf{k}\mathbf{k}'}$, and λ is the eigenvalue. For $\chi > 0$, the critical temperature is given by $k_B T_c = 1.14\epsilon_c e^{-1/\chi}$. For $\chi \le 0$, the eigenvector $\Psi(\mathbf{k})$ is not a pairing instability. The most favorable pairing function $\Delta(\mathbf{k})$ is proportional to the eigenvector $\Psi(\mathbf{k})$ with the largest positive eigenvalue χ.

Fig.3a shows a phase diagram with respect to $J_x = J_y = J$ and V_0, where we have fixed $V_x = V_y = V < 0$. Different phases are distinguished by the topology of their nodal lines, and are labeled using different Greek letters. Both the α phase and the α' phase are double-helix nodal-line phases with different double helix helicities. The typical nodal-line shapes of the α and α' phases are shown in Fig.3b and 3c, respectively, where $\theta = \arg(\widetilde{k}_x + ik_y)$ is the poloidal angle of the torus fermi surface. Fig.3e shows the double-helix nodal lines of the α phase in the 3d BZ. We note that the physical picture in Fig.2 only predicts the double-helix helicity of phase α, which is valid for small λ_z/λ [29]. In the case we calculated in Fig.3 where λ_z/λ is large, both phases α and α' arise, which is because the projected interaction in Eq.(6) in this case does not give a double-helix helicity preference. The β phase has two unlinked nodal loops as shown in Fig.3d, while the γ phase is fully gapped without any nodal lines. The phase diagram shows that ferromagnetic spin interactions $J < 0$ tend to favor double-helix nodal lines, which makes η_1 and η_2 positive as required in our argument. We note that ferromagnetic electron interactions are quite common for metals.

We have seen that the realization of linked nodal lines requires torus or higher genus fermi surfaces, and strongly varying spin textures along the toroidal direction of the fermi surfaces. These conditions put a limitation on the crystalline symmetry of candidate materials. In general, a lower crystalline symmetry is preferred. In particular, in the double helix nodal line configuration in Fig.1a, the only allowed point-group symmetry (up to a translation) is either a two-fold rotation C_{2x} about x axis or a mirror reflection M_x from x to $-x$. In other configurations as shown Fig.1b-d, a few other symmetry operations such as the three-fold rotation C_{3z} are allowed. For instance, the configuration of Fig.1c is allowed for materials with a hexagonal 3R structure, which is common in transition metal dichalcogenides[31]. We therefore suggest to search for (double-helix) linked nodal-line superconductors in layered metallic materials with strong SOCs and low crystalline symmetries, such as lithium-inserted metal oxide, transition metal dichalcogenides and transition metal halides,

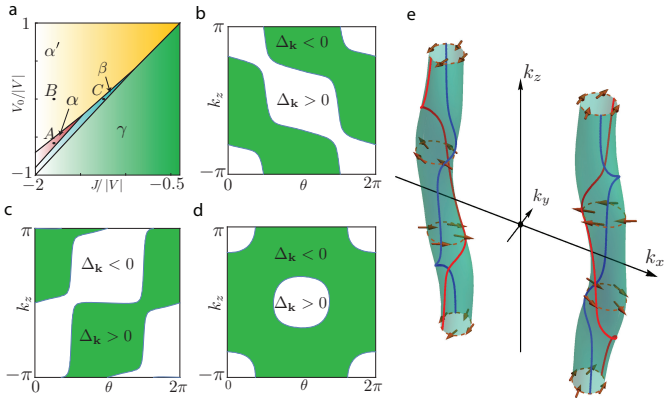

FIG. 3: **a**. Phase diagram for fixed $V < 0$, where the horizontal and vertical axes are J and V_0, respectively. Both α and α' phases are double-helix linked nodal line phases, except that their helicities are opposite. The β phase contains two unlinked nodal lines on each fermi surface. The γ phase is the conventional fully gapped phase. Panels **b**-**d** show the nodal-line configuration on the fermi surface at $k_x = \pi/2$ for points A, B and C in the phase diagram, respectively, where $\theta = \arg(\widetilde{k}_x + ik_y)$ is the poloidal angle of the torus fermi surface. **e**. The 3d plot of the spin texture (arrows) and nodal lines (blue and red lines) on the fermi surfaces at point A of the phase diagram.

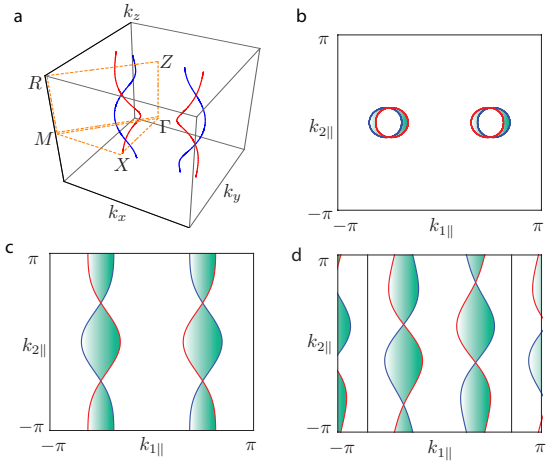

FIG. 4: **a**. Sketch of a typical example of double-helix nodal lines in the BZ. **b**-**d**. Illustration of the zero-energy surface Majorana flat bands (colored in green) on surface cuts along Γ-Z, Γ-X and Γ-M directions, which are bounded by the projection of nodal lines.

etc[32], where torus fermi surfaces and strongly varying spin textures are more likely to occur.

The detection of linked nodal lines is also essential in experiments. A few techniques such as corner junction [2, 33], angular-resolved thermal transport measurement [34, 35] and angular-resolved photoemission spectroscopy (ARPES)[6] have been used to reveal the nodal structure of superconductors, which will, however, be more complicated for linked nodal lines. Instead, we suggest a possibly easier way to reveal linked nodal lines through probing the surface states on the surface cuts of different directions using ARPES. As we mentioned at the beginning, nodal line superconductors exhibit topologically protected zero energy Majorana flat bands, which are bounded by the projection of nodal lines on the surface [17–19]. If two nodal lines are linked, their projections will necessarily cross each other on any surface cuts. Therefore, the corresponding surface Majorana flat bands always kiss each other as shown in Fig.4, no matter which surface cut one takes.

In conclusion, we have demonstrated the possibility of realizing linked nodal lines in noncentrosymmetric superconductors with torus or higher genus fermi surfaces and strongly **k**-dependent spin textures, and studied an explicit lattice model that realizes a double-helix nodal-line superconductor. These results may serve as a preliminary guidance on searching for and detecting linked nodal-line superconductors in nature.

Acknowledgements: We are grateful to Peizhe Tang for helpful discussions. This work is supported by the NSF grant DMR-1305677.

[1] C.-R. Hu, Phys. Rev. Lett. **72**, 1526 (1994).
[2] D. A. Wollman, D. J. Van Harlingen, W. C. Lee, D. M. Ginsberg, and A. J. Leggett, Phys. Rev. Lett. **71**, 2134 (1993).
[3] D. A. Wollman, D. J. Van Harlingen, J. Giapintzakis, and D.M. Ginsberg, Phys. Rev. Lett. **74**, 797 (1995).
[4] J. Kirtley, C. Tsuei, J. Sun, C. Chi, et al., Nature **373**, 225 (1995).
[5] K. Okazaki, Y. Ota, Y. Kotani, W. Malaeb, Y. Ishida, T. Shimojima, T. Kiss, S. Watanabe, C.-T. Chen, K. Kihou, et al., Science **337**, 1314 (2012).
[6] Y. Zhang, Z. Ye, Q. Ge, F. Chen, J. Jiang, M. Xu, B. Xie, and D. Feng, Nat. Phys. **8**, 371 (2012).
[7] E. Bauer, G. Hilscher, H. Michor, C. Paul, E. W. Scheidt, A. Gribanov, Y. Seropegin, H. Noël, M. Sigrist, and P. Rogl, Phys. Rev. Lett. **92**, 027003 (2004).
[8] S. Yip, Annu. Rev. Condens. Matter Phys. **5**, 15 (2014).
[9] B. Lian, C. Vafa, F. Vafa, and S.-C. Zhang, Phys. Rev. B **95**, 094512 (2017).
[10] W. Chen, H.-Z. Lu, and J.-M. Hou, Phys. Rev. B **96**, 041102 (2017).
[11] Z. Yan, R. Bi, H. Shen, L. Lu, S.-C. Zhang, and Z. Wang, Phys. Rev. B **96**, 041103 (2017).
[12] M. Ezawa, Phys. Rev. B **96**, 041202 (2017).
[13] Z. Wang, X.-L. Qi, and S.-C. Zhang, Phys. Rev. B **84**, 014527 (2011).
[14] S. Ryu, J. E. Moore, and A. W. W. Ludwig, Phys. Rev. B **85**, 045104 (2012).
[15] A. M. Polyakov, Mod. Phys. Lett. A **3**, 325 (1988).
[16] E. Witten, Commun. Math. Phys. **121**, 351 (1989).
[17] A. P. Schnyder and S. Ryu, Phys. Rev. B **84**, 060504 (2011).
[18] A. P. Schnyder, P. M.R. Brydon, and C. Timm, Phys. Rev. B **85**, 024522 (2012).
[19] A. P. Schnyder and P. M.R. Brydon, J. Phys. : Condensed Matter **27**, 243201 (2015).
[20] M. Sato, Y. Tanaka, K. Yada, and T. Yokoyama, Phys. Rev. B **83**, 224511 (2011).
[21] Y. Tanaka, M. Sato, and N. Nagaosa, J. Phys. Soc. Jpn **81**, 011013 (2011).

[22] J. D. Watson and F. H. Crick, Nature **171**, 737 (1953).
[23] J. Watson, *The double helix* (Hachette UK, 2012).
[24] P. W. Anderson, Phys. Rev. B **30**, 4000 (1984).
[25] X.-L. Qi, T. L. Hughes, S. Raghu, and S.-C. Zhang, Phys. Rev. Lett. **102**, 187001 (2009).
[26] C. Gauss, *Werke, vol. 5 (göttingen, 1867)*.
[27] M. Sigrist and K. Ueda, Rev. Mod. Phys. **63**, 239 (1991).
[28] P. A. Frigeri, D. F. Agterberg, A. Koga, and M. Sigrist, Phys. Rev. Lett. **92**, 097001 (2004).
[29] See supplemental online material for more details.
[30] M. Sigrist, AIP Conf. Proc. **789**, 165 (2005).
[31] M. Chhowalla, H. S. Shin, G. Eda, L.-J. Li, K. P. Loh, and H. Zhang, Nat. Chem. **5**, 263 (2013).
[32] P. Miró, M. Audiffred, and T. Heine, Chem. Soc. Rev. **43**, 6537 (2014).
[33] D. Van Harlingen, Rev. Mod. Phys. **67**, 515 (1995).
[34] M. J. Graf, S. K. Yip, J. A. Sauls, and D. Rainer, Phys. Rev. B **53**, 15147 (1996).
[35] Y. Matsuda, K. Izawa, and I. Vekhter, J. Phys.: Condensed Matter **18**, R705 (2006).